Astronomy & Astrophysics

Photospheric and coronal magnetic fields in six magnetographs

II. Harmonic scaling of field intensities

Ilpo Virtanen and Kalevi Mursula

ReSoLVE Centre of Excellence, Space Climate research unit, University of Oulu, PO Box 3000, 90014 Oulu, Finland
e-mail: [ilpo.virtanen;kalevi.mursula]@oulu.fi

ABSTRACT

Context. Photospheric magnetic fields have been observed since the 1970s by several ground-based and satellite instruments. While the different instruments show a fairly similar large-scale structure and temporal evolution of the photospheric magnetic field, the magnetic field intensity varies significantly between the observations.

Aims. We introduce a new method for scaling the photospheric magnetic field in terms of the harmonic expansion. Contrary to earlier scaling methods, the harmonic scaling method can be straightforwardly used for data sets of different resolutions.

Methods. We use synoptic maps constructed from Wilcox Solar Observatory, Mount Wilson Observatory (MWO), Kitt Peak (KP), SOLIS, SOHO/MDI and SDO/HMI measurements of the photospheric field. We calculate the harmonic expansions of the magnetic field for all these data sets (for most, up to $n = 180$) and investigate the scaling of the harmonic coefficients between all possible pairs of data sets.

Results. The six data sets generally scale to one another relatively well, with the exception of even axial terms, especially the g_2^0 quadrupole for a few pairs of data sets. Differences in polar field observations, pole-filling methods and possible zero-level mainly affect the scaling of even axial terms. Scaling factors typically slightly increase with harmonic order. The mutual scaling between SOLIS and HMI is very good, and one single overall coefficient of approximately 0.8 would be a reasonable choice for those data sets. Our results suggest that the KP synoptic maps are offset by a few degrees with respect to MWO and MDI. We note that the new method gives a correct scaling for the low harmonic terms that are sufficient and necessary for coronal modeling.

Key words. Sun: magnetic fields – Sun: photosphere – Sun: activity

1. Introduction

The large-scale solar magnetic field has been measured since the 1950s (Babcock 1953), but a continuous series of calibrated digital magnetic field data exist only since the 1970s. During these 60 yr the observation techniques, as well as the computational resources for data processing and storage have dramatically improved. However, these changes have led to a number of inhomogeneities in most observational data sets.

Observations of sunspot magnetic fields started in Mount Wilson Observatory (MWO) already in the early 1900s (Hale 1908), but full-disk observations of large-scale magnetic fields became possible only in the 1950s after the invention of diode light detectors. Various instrumentation and data-storage systems were used during the first decades of full-disk observations of MWO. Data storage became digital in 1967 and routine daily observations started in the early 1970s. MWO magnetograph observations were terminated in January 2013.

Observations of the photospheric magnetic field started in Kitt Peak (KP) observatory in 1970 and were carried out over four decades, until the relocation of the Synoptic Optical Long-term Investigations of the Sun (SOLIS) magnetograph away from Kitt Peak in 2014. Wilcox Solar Observatory (WSO) observations started in 1976 and the WSO magnetograph has been operating since then without major updates. The first satellite magnetograph, Michelson Doppler Imager (MDI) on board SOHO spacecraft started observations in 1996 and was succeeded by the Helioseismic and Magnetic Imager (HMI) on board the SDO satellite in 2010.

Different data sets indicate a fairly similar large-scale structure and long-term evolution of the photospheric magnetic field. Also the hemispherical asymmetry of the photospheric field and the related PFSS coronal field appear very consistently in all observations (Virtanen & Mursula 2016, hereafter referred to as Paper I). However, the overall intensity of the magnetic field greatly differs between the data sets. Partly these differences relate to the known observational differences but, overall, the intensity differences between the data sets cannot be explained very well. Therefore, scaling factors are needed when comparing magnetic field intensities from different instruments (see, e.g., Pietarila et al. 2013; Riley et al. 2014, and references therein).

There are several known effects causing differences between instruments: atmospheric effects, telescope optics, magnetograph instrumentation, spectral line selection, spatial and spectral resolutions, integration time, data processing, and so on. Differences between the data sets may also vary in time and depend, for example, on the phase of the solar cycle. Instrument updates may also have a significant effect on relative scaling. Several studies have compared the line-of-sight full-disk magnetograms, mostly between two data sets (Pietarila et al. 2013; Tran et al. 2005; Berger & Lites 2003; Liu et al. 2012). The most straightforward method to compare two data sets is pixel-by-pixel comparison, where simultaneous full-disk observations are

first averaged to same resolution and then the magnetic flux densities in corresponding pixels are compared pixel-by-pixel.

Pixel-by-pixel comparisons have shown (Tran et al. 2005; Berger & Lites 2003) that scaling is, in general, nonlinear, the slope of the regression line between two data sets depending on the magnetic field intensity and solar cycle phase. A critical issue with pixel-by-pixel comparison is that scaling factors depend on the resolution of data. The spatial resolution of instrumentation is known, but the varying seeing conditions in ground-based observations affect the effective spatial resolution, but cannot easily be taken into account (Pietarila et al. 2013).

An alternative to the pixel-by-pixel comparison is to find an average scaling between disk-averaged magnetic field intensities using several pairs of simultaneous observations. The benefit of disk-average comparison is that it is independent of resolution and can be directly applied for comparing any pair of full-disk line-of-sight observations. However, the disadvantage is that disk-averaging neglects possible nonlinearities in scaling. Pixel-by-pixel and disk-average comparisons between two data sets that are carried out roughly at the same resolution typically agree reasonably well with each other.

Synoptic maps constructed using data from WSO, MWO, KP, GONG (Global Oscillation Network Group), SOLIS, MDI and HMI have also been compared in detail (Riley et al. 2014). As they described, there is no "ground truth" in the intensity of the photospheric magnetic field; the overall intensity of the photospheric field tends to vary between the data sets. Scaling factors between synoptic data sets depend on time, field intensity, and latitude. The method of constructing the synoptic map and the possible filling of polar fields in synoptic maps also cause differences between the data sets, in addition to the above mentioned differences between the full-disk magnetograms. Moreover, observation of the corresponding pixels of the synoptic maps were not carried out exactly simultaneously by the different instruments. There are also non-simultaneous gaps in the data sets. Therefore all pixels in the synoptic maps do not necessarily represent exactly simultaneous observations, nor exactly the same region of the solar surface.

The observed photospheric magnetic field is used as the inner boundary condition for coronal magnetic field models. Coronal magnetic field, on the other hand, defines the structure of the modeled heliospheric magnetic (HMF) field. Unfortunately, the coronal magnetic field cannot be directly measured yet. Models of the coronal magnetic field (Altschuler & Newkirk 1969; Schatten et al. 1969; Hoeksema et al. 1983), solar wind (Arge & Pizzo 2000; Arge et al. 2010) and the heliospheric magnetic field are urgently needed for space weather and space climate studies. The question of the correct scaling of the photospheric magnetic field is highly important for these models and their correspondence with the observed properties of the solar wind and the HMF.

The aim of this article is to compare the intensity of the photospheric magnetic field at WSO, MWO, KP, SOLIS, MDI and HMI. As described above, several preceding studies concluded that scaling is nonlinear and depends on resolution, latitude and time. Instead of comparing the different full-disk magnetograms or synoptic maps either pixel-by-pixel or by their disk-averaged values, we study here the scaling needed for coefficients of the harmonic expansions of the different data sets. This is a more proper approach from the heliospheric point of view, since the coronal magnetic field and the heliospheric magnetic field can be described by using only a few of the lowest multipole terms of the harmonic expansion (Wang 2014; Koskela et al. 2017).

The paper is organized as follows: in Sects. 2 and 3 we present the data and methods used in this work, respectively. Section 4 shows our results on scaling between WSO and other data sets and Sect. 5 gives the results on scaling between the other six pairs of data sets. Section 6 presents our results for higher harmonic scaling. We discuss our results in more detail in Sect. 7 and give our final conclusions in Sect. 8.

2. Data

2.1. Instruments and data sets

The longest homogeneous series of observations of the photospheric magnetic field is from the WSO, where essentially the same instrumentation has been operating since 1976. Although the WSO magnetograph is a low-resolution device (3 arcmin aperture size), which suffers from saturation (Svalgaard et al. 1978), WSO observations give us essential information about solar magnetic fields over long timescales of several solar cycles. Daily observations of the photospheric field started at the MWO already in 1959, but data has been calibrated to uniform digital format only since 1974. There were major instrumental updates at MWO in 1982, 1994, and 1996, before MWO observations were terminated in January 2013. The KP observatory started observing photospheric fields in 1970, first using a 40-channel photoelectric magnetograph, then since 1974 a 512-channel magnetograph and since 1992 a spectromagnetograph. KP spectromagnetograph was succeeded by SOLIS in 2003. We neglect KP data before 1992, when there were serious problems in synoptic maps (Harvey & Munoz-Jaramillo 2015; Virtanen & Mursula 2016). The MDI instrument on board the SOHO spacecraft was operational between 1996 and 2011. It was the first satellite magnetograph and allowed continuous observations of the photospheric magnetic field without the distorting effect of the Earth's atmosphere. MDI was succeeded by the HMI instrument on board the SDO satellite in 2010, with a short overlapping period to allow calibration between these two instruments. Besides the traditional line-of-sight component, HMI and SOLIS are able to measure the full three-dimensional vector magnetic field.

Table 1 shows the time spans and the resolutions of the synoptic maps, as well as the measured spectral lines of the six data sets used in this work. The data sets are obtained by six different instruments using mostly different spectral lines, telescope properties, and spatial and spectral resolutions. They also use different methods to calculate the magnetic field from instrument signal. We note that the spatial resolution of WSO and MWO observations is lower than the resolution of the corresponding synoptic maps. WSO aperture size is 3 arc-min, which means approximately 33 pixels in longitude in the equator. The aperture in MWO was a square of either 12.5 or 20.0 arc-sec, which corresponds to roughly 480/300 pixels in the full equatorial longitude range.

We use synoptic maps in their original published format without any modifications. WSO, KP, SOLIS, MDI and HMI data are given in longitude – sine-latitude grid, which makes the cell size constant. In MWO the grid of the synoptic map is linear in latitude and the cell size decreases with latitude. The varying cell size at MWO is taken into account by weighting the cell value by the area (cosine of latitude) when calculating harmonic coefficients (see later). Since scaling is sensitive to data gaps, we use only 100% full maps without any gaps. This requirement decreases data especially at WSO, where some data gaps exist every year, especially in winter months when seeing is poorest.

Table 1. Properties of synoptic map data sets used in this study.

Data set	Spectral line	Time span	Carrington rotations	Map resolution
WSO	Fe 525 nm	1976.3–	1641–	72*30
MWO	Fe 525 nm	1974.5–2013.0	1617–2131	971*512
Kitt Peak	Fe 868.8 nm	1992.8–2003.7	1863–2006	360*180
SOLIS	Fe 630.2 nm	2003.7–	2006–	1800*900
MDI	Ni 676.8 nm	1996.4– 2011.1	1909–2104	3600*1080
HMI	Ni 617.3 nm	2010.4–	2096–	3600*1440

Notes. Map resolution stands for the number of pixels in longitude and latitude. Grid is linear in latitude in the MWO data set and linear in sine latitude in other data sets.

The number of data gaps decreases if observations with a larger longitudinal offset from central meridian are used. The maximum offset allowed when constructing the synoptic maps from full-disk observations varies between the data sets.

In Paper I we noted that WSO data is erroneous during rotations 1905–1944 (decimal years 1996.0–1999.0) and rotations 1973–1978 (2001.1–2001.5). We neglect these periods in this work since errors affect scaling essentially, and including these periods would significantly affect the results. In Paper I we also neglected SOLIS data before March 2006 (CR 2040) because of inhomogeneous calibration. However, SOLIS data were recalibrated in 2016 (priv. comm. with Luca Bertello/NSO SOLIS team), which allows us to now use the whole SOLIS data set from 2003 onwards.

2.2. Polar fields

Polar fields are difficult to observe for several reasons. First of all, polar fields are often rather weak. The average polar field (radial B_r) intensity at WSO during the declining phase of solar cycles 21 and 22 was approximately 0.5 mT and during the declining phase of solar cycle 23 it was only approximately 0.3 mT. The noise level in WSO line-of-sight observations of the photospheric magnetic field is less than 0.01 mT (Hoeksema 1985), which corresponds to approximately 0.04 mT noise level for radial field in the highest pixels centered at 75.2° latitude. Other instruments typically show larger polar field intensities than WSO but, due to higher spatial resolution, they also have a lower signal-to-noise ratio. For example, SOLIS radial polar field intensity[1] during solar cycle 23 minimum was roughly 0.4 mT, while SOLIS noise level for line-of-sight observations is roughly 0.1 mT (priv. comm. with SOLIS team). This corresponds to roughly 0.2 mT–0.4 mT noise level for radial field in 60°–75° latitude band in SOLIS. Moreover, satellite magnetographs have a much higher noise level. The noise level in MDI line-of-sight observations is 2.6 mT and in HMI 1 mT (Liu et al. 2012). This means that polar field intensity can be below the instrument noise level in high-resolution data sets. Second, since the ecliptic plane is tilted by 7.25° (the so-called b_0 angle) with respect to solar equatorial plane, the two solar poles are not simultaneously visible during most of the year. Third, the measured line-of-sight component is almost perpendicular to the roughly radial field at the highest latitudes, making the measurements less reliable with increasing latitude due to this projection effect and due to related increase of the relative noise level of the solar atmosphere. Therefore the synoptic maps suffer from systematic limitations that have to be appropriately taken into account.

In WSO data the pixel size is so large that the highest pixel of synoptic maps (68.9°–90°, centered at 75.2°) includes the polar area and no polar field filling is needed. MWO and HMI synoptic maps include only the measured regions up to the annually varying maximum latitude, and no polar field filling is used. Kitt Peak maps have been filled for the polar fields using cubic spline fitting, and SOLIS polar fields are filled using a cubic-polynomial fit to the observed fields at neighboring latitudes. MDI maps have also been filled for polar fields (Sun et al. 2011). Paper I discusses in more detail the different ways to treat polar fields in these six data sets. Petrie (2015) also compare different methods of polar field filling.

The annually varying b_0 angle and the related effects discussed above cause an annual oscillation in the observations of the photospheric magnetic field. This effect is often called the vantage point effect (or the b_0 angle effect) and it appears in a different way in the six data sets. It is most obvious in MWO and WSO synoptic maps, where the polar field of the pole with better visibility has a systematically larger intensity. A similar but weaker b_0 angle effect is also seen in KP, SOLIS, and MDI synoptic maps (Paper I). The vantage point effect appears very weakly, if at all, in HMI synoptic maps (Upton & Hathaway 2014, Paper I). Ulrich & Tran (2013) suggested that the vantage point effect relates to a systematic poleward tilt of the polar fields, which decreases the intensity of the observed line-of-sight component of the photospheric magnetic field. They used a latitude dependent correction ζ, which increases field intensities especially at the less visible pole, when the magnetic field is almost perpendicular to the line-of-sight. Their method significantly reduces the annual oscillation in high-latitude field intensities at MWO. However, it has not been verified that the magnetic field is indeed tilted poleward at high latitudes. The vantage point effect also depends on spatial resolution, and on the way the polar field filling is made. It may also depend on other factors such as the noise level of high-latitude measurements, integration time of observations, or the calculation of field intensity using different spectral lines.

3. Methods

Several methods have been used to compare the different observations of the photospheric field to one another, but no method gives an unambiguous relation between any two data sets. As described, for example, by Riley et al. (2014), the high-resolution synoptic maps, when averaged to a lower resolution, are different from maps that are originally measured in low resolution. This is at least partly due to the fact that averaging pixels of a synoptic map averages over magnetic field values, but measuring the average field of the larger region averages over the spectral line profiles, and the response is different. Averaging

---

[1] http://solis.nso.edu/0/vsm/vsm_plrfield.html

of a high-resolution map should represent the average magnetic field better but, on the other hand, measuring over a larger region gives a better signal to noise ratio.

The way the observed photospheric magnetic field element contributes to the coronal and heliospheric fields depends on latitude and solar cycle phase. During the declining to minimum phase of the solar cycle the polar fields are the most important factor defining the structure of coronal and heliospheric magnetic fields. That is why it is essential to have a correct scaling also for polar fields.

Polar field area is relatively small. Polar caps from 60° to 90° in the two hemispheres cover only 13% of the total solar surface, and a significant fraction of polar caps is often invisible due to the vantage point effect. Moreover, polar cap field is never unipolar in high-resolution observations, even though one polarity appears more often around one pole than the another. Pietarila et al. (2013) showed that the weak fields of SOLIS full-disk magnetograms ($|B| < 3$ mT) are mainly dominated by noise, and that the scaling factors are very different for weak and strong fields. This suggests that polar fields are easily masked by noise in statistical analyses of full-disk magnetograms or synoptic maps. That is why we do not use scaling methods that aim to find the best overall agreement between full-disk observations or synoptic maps of different data sets, since those methods do not pay attention to the special role of polar fields.

3.1. Multipole expansion

The assumption that the magnetic field inside the solar corona is current-free and stationary leads, together with Maxwell equations, to a Laplace equation for the magnetic scalar potential, which can be solved in terms of spherical harmonics. A commonly used solution is the potential field source surface (PFSS) model of the coronal magnetic field, which was first implemented already more than 40 years ago (Altschuler & Newkirk 1969; Schatten et al. 1969; Hoeksema et al. 1983). The PFSS model assumes that, at a certain distance called the source surface (r_{ss}), the radially out-flowing plasma takes over the magnetic field and the field becomes radial. Thereby the outer boundary condition requires that the field is radial at r_{ss}. The PFSS solution for the radial component of the coronal field from the photosphere to the source surface is

$$B_r(r, \theta, \phi) = \sum_{n=1}^{n_{max}} \sum_{m=0}^{n} P_n^m(\cos\theta)(g_n^m \cos m\phi + h_n^m \sin m\phi)C(r, n), \quad (1)$$

where the radial functions $C(r, n)$ are

$$C(r, n) = \left(\frac{R}{r}\right)^{n+2} \left[\frac{n + 1 + n\left(\frac{r}{r_{ss}}\right)^{2n+1}}{n + 1 + n\left(\frac{R}{r_{ss}}\right)^{2n+1}}\right], \quad (2)$$

and $P_n^m(\cos\theta)$ are the associated Legendre functions, R is the solar radius, r is the radial distance and θ is the co-latitude (polar angle). Here we neglect the nonphysical magnetic monopole term ($m = n = 0$) by starting from $n = 1$.

The harmonic coefficients g_n^m and h_n^m of the expansion (1) are obtained from the synoptic maps of the observed photospheric magnetic field. When the map is given in the longitude – sine-latitude grid, the harmonic coefficients g_n^m and h_n^m are as follows:

$$\left\{ \begin{matrix} g_n^m \\ h_n^m \end{matrix} \right\} = \frac{2n + 1}{N} \sum_{i=1}^{N_\theta} \sum_{j=1}^{N_\phi} \frac{B_{j,i}^{los}}{\sin\theta_i} P_n^m(\cos\theta_i) \left\{ \begin{matrix} \cos(m\phi_j) \\ \sin(m\phi_j) \end{matrix} \right\}, \quad (3)$$

where $B_{j,i}^{los}$ refers to the measured photospheric line-of-sight value at longitude – sine-latitude bin (j, i), N_ϕ is the number of data bins in longitude, and N_θ is the number of data bins in latitude and $\sin(\theta_i)^{-1}$ term comes from the assumption that the photospheric magnetic field is radial. N is the number of existing data points in the grid ($N = N_\theta N_\phi$ if no data gaps exist). The solid angle covered by each cell is constant $\Delta\Omega = 4\pi/N_\phi N_\theta$.

When the measured data is given in the longitude-latitude grid, the bin area decreases with latitude and solid angle $\Delta\Omega = \sin\theta\Delta\theta\Delta\phi$, where $\Delta\theta = \pi/N_\theta$ and $\Delta\phi = 2\pi/N_\phi$. In this case the harmonic coefficients are as follows:

$$\left\{ \begin{matrix} g_n^m \\ h_n^m \end{matrix} \right\} = \frac{\pi}{2} \frac{2n + 1}{N} \sum_{i=1}^{N_\theta} \sum_{j=1}^{N_\phi} B_{j,i}^{los} P_n^m(\cos\theta_i) \left\{ \begin{matrix} \cos(m\phi_j) \\ \sin(m\phi_j) \end{matrix} \right\}. \quad (4)$$

The large-scale coronal magnetic field at the source surface and the HMF further out can be described by using only a few of the lowest multipole terms (Wang 2014; Koskela et al. 2017). However, here we also include higher harmonic terms, since they contribute to the differences between the data sets (in the photosphere) and also affect the coronal magnetic field configuration inside the source surface.

Nyqvist theorem gives the limit for the highest possible term in the harmonic expansion (1). According to Eq. (3) the limit in longitude gives $n_{max} < N_\phi/2$ (assuming that the observational resolution is at least as high as in the synoptic map). The Legendre polynomial P_n^m is zero along $n - m$ circles of constant latitude and $\sin m\phi$ and $\cos m\phi$ terms in Eq. (3) are zero along $2m$ circles of constant longitude. Thereby the axial $m = 0$-terms and the latitudinal resolution of high latitude observations define the highest possible multipole n_{max} in latitude direction.

In the case of WSO, which has the lowest resolution, the aperture size is 3 arcmin, corresponding to approximately 33 pixels in longitude (in the equator), where $n_{max} = 16$. In latitude the polemost 3 arcmin covers roughly 35° from the pole, which would allow to solve the coefficients only up to $n_{max} = 2$. The second highest latitude band (40°–55°) would allow roughly $n_{max} = 6$, and in the equator $n_{max} = 16$ is sufficient. Overall, we consider that $n_{max} = 9$, which is also used for published WSO coronal maps, is a reasonable choice for the harmonic expansion, even for the low-resolution data of WSO.

3.2. Linear fitting

We determine the scaling factor between any two time series by linear fitting. The most traditional way to complete linear fit is the least squares fitting, where the best fit line is defined by minimizing the sum of squared vertical offsets of points from the line. Here we attempt to find a fit which is unambiguous in terms of fitting X_1 versus X_2 or X_2 versus X_1, that is, the scaling factor between the two data sets should be symmetric. We note that neither X_1 nor X_2 is exactly known and their errors are typically also unknown but roughly of the same order of magnitude. We use a method which minimizes the sum of squared perpendicular distances of points from the line. This is carried out by the singular value decomposition (SVD), which solves the principal components of the two data sets, the first principal component being the best linear fit between X_1 and X_2.

In general, if X is an $m \times n$ real matrix with $m > n$, then it can be expressed in terms of a singular value decomposition as follows:

$$X = USV^T, \quad (5)$$

where S is a diagonal matrix with decreasing (absolute) values from λ_1 to λ_n. In our case X is $m \times 2$ matrix, where the two columns are rotational values of harmonic coefficients derived from two data sets. Thereby U is $m \times 2$, S is 2×2 and V is 2×2 matrix.

The two principal components of X are the columns of matrix $P = US$, and the original variable X is the linear combination $X_{\{i\},j} = P_{\{i\},1}V_{j,1} + P_{\{i\},2}V_{j,2}$. The first principal component $P_{\{i\},1}$ describes the best (linear) fit between two columns of matrix X and the second principal component $P_{\{i\},2}$ the deviations from the best-fit line. Thereby the slope of the linear fit $X_{\{i\},2} = kX_{\{i\},1}$ is

$$k = \frac{V_{2,1}}{V_{1,1}}. \tag{6}$$

The method is described in more detail by, for example, Jolliffe (2005) and Holappa et al. (2014).

Error estimates are calculated in the following way. As mentioned above, $P_{\{i\},2}V_{j,2}$ give the residuals. We shuffle the residuals and construct a new data set $X_{\{i\},j}^r = P_{\{i\},1}V_{j,1} + P_{\{k\},2}V_{j,2}$, where index k goes through the same values as i, but in a random order. We repeat the analysis and calculate the singular value decomposition using $X_{\{i\},j}^r$ and obtain a new slope k^r. This procedure is repeated m*100 times, and gives us the distribution of slopes k^r, which allows us to define the 2σ errors (95% confidence intervals). The method is probably slightly affected by the autocorrelation of residuals, which mainly relates to the varying size of the b_0 effect in different data sets. This indicates that errors are not completely randomly distributed, and a more realistic distribution would probably make the errors somewhat larger.

4. Scaling of the first two harmonics between WSO and MWO

4.1. Coefficients of the lowest harmonics

Figure 1 shows the coefficients of the four lowest terms of the harmonic expansion, the axial dipole g_1^0, the axial quadrupole g_2^0 and the two equatorial dipoles g_1^1 and h_1^1 in absolute scale (units of μT) for the six data sets. Panels on the left show the rotational values and panels on the right the 13-rotation running means. As already evidenced by previous studies (see above discussion), the different data sets behave in a broadly similar fashion, although occasional deviations are found. Note that the values of the coefficients in Fig. 1 are based on the original non-scaled synoptic maps, and no scaling has been applied yet.

The axial dipole term g_1^0 shows the well known 22-yr solar magnetic cycle, reaching its maxima and minima in the declining to minimum phase of the solar cycle. The axial dipole term is typically smallest in WSO, systematically larger in MWO and largest in KP in 1992–2003. MDI depicts slightly smaller values than KP during their overlapping period. After 2003 g_1^0 is typically largest in SOLIS and slightly smaller in MDI (2006–2010) and in HMI (2010–). The level of annual oscillation is very low in g_1^0 term, and appears only in early MWO data.

The g_2^0 quadrupole term depicts a fairly strong annual oscillation in most databases. The annual oscillation has its maximum and minimum values when the Earth is at the highest northern or southern heliographic latitudes (in spring or fall), that is, when the visibility of the solar polar regions is most unbalanced. However, interestingly, this vantage point effect appears in a different way in the different data sets. The annual oscillation is most strongly and most systematically present in MWO data and

in early WSO data. Both data sets indicate that the magnitude of southern (northern) polar field is systematically larger during spring (fall), when the visibility of the respective pole is at maximum. However, in KP and SOLIS data, the annual oscillation of the g_2^0 term has an opposite phase. This indicates that the polar field-filling method used in KP and SOLIS data leads to a larger polar field magnitude at the pole which is filled than at the opposite, more visible and better observed pole. This leads to some doubts about the validity of the filling method in KP and SOLIS data. On the other hand, there is hardly any annual oscillation in MDI data, indicating a better success of the polar filling method (Sun et al. 2011). We also find only a weak annual oscillation in the g_2^0 term in HMI, even though invisible poles are not filled in HMI synoptic maps.

As found earlier (Zhao et al. 2005; Virtanen & Mursula 2014, Paper I) the g_2^0 term has an average positive level during the declining to minimum phase in the 1980s and a negative level in the 1970s and 1990s, that is, opposite to the sign of the simultaneous g_1^0 term, leading to the systematic southward shift of the HCS (Mursula & Hiltula 2003). Like the axial dipole term, the absolute value of the g_2^0 term is also somewhat smaller in WSO than in MWO (see the 13-rotation plots of Fig. 1). The $|g_2^0|$ is largest in KP in 1992–1996 and in MDI in 1996–2003. During the late declining to minimum phase of SC23, the g_2^0 term is consistently smaller than during corresponding times of earlier cycles, and the expected positive dominance (most clearly seen in SOLIS) is intervened by negative values in 2005–2006, making the HCS southward shift less systematic during this cycle (Mursula & Virtanen 2011; Virtanen & Mursula 2014). Still, all data sets produce a very similar evolution for g_2^0 even during this time. The fast increase of g_2^0 after 2010, as well as its fast decrease to large negative values since 2013 is seen in all available data sets. WSO shows again the smallest absolute values, MWO slightly larger, and HMI and SOLIS the largest values.

The equatorial dipole terms g_1^1 and h_1^1 reach their largest (absolute) values around solar maxima and the smallest (absolute) values during solar minima, in phase with the solar cycle variation of the production rate of new active regions. A particularly long period of weak values of g_1^1 and h_1^1 is found around the latest solar minimum in 2007–2009, which was exceptionally long and deep in many measures of solar activity (Schrijver & Liu 2008; Lefèvre & Clette 2011; Livingston & Penn 2009; Muñoz-Jaramillo et al. 2015). WSO and MWO depict very similar values of g_1^1 and h_1^1 over the whole time interval, MWO being typically slightly larger, but not always. KP values of g_1^1 and h_1^1 are considerably larger than for WSO and MWO, and after 1996 agree very well with MDI. SOLIS shows the largest values also for g_1^1 and h_1^1 from 2003 onward, while HMI values are typically smaller than SOLIS, but larger than others.

4.2. Scaling of low harmonics between WSO and MWO

The left panels of Fig. 2 illustrate the method of deriving the best linear scaling factors from WSO to MWO for harmonic coefficients g_1^0, g_2^0, g_1^1 and h_1^1. The right side panels show original coefficients for WSO (partly reproducing Fig. 1) and rotational harmonic coefficients for MWO scaled to WSO level for those rotations where both data sets have a synoptic map which fulfills the data coverage requirements. Figure 2 shows that the g_1^0 term scales fairly uniformly between WSO and MWO. The average slope of the linear regression, for example, the scaling factor from WSO to MWO, is 1.43 and the estimated 2σ error is
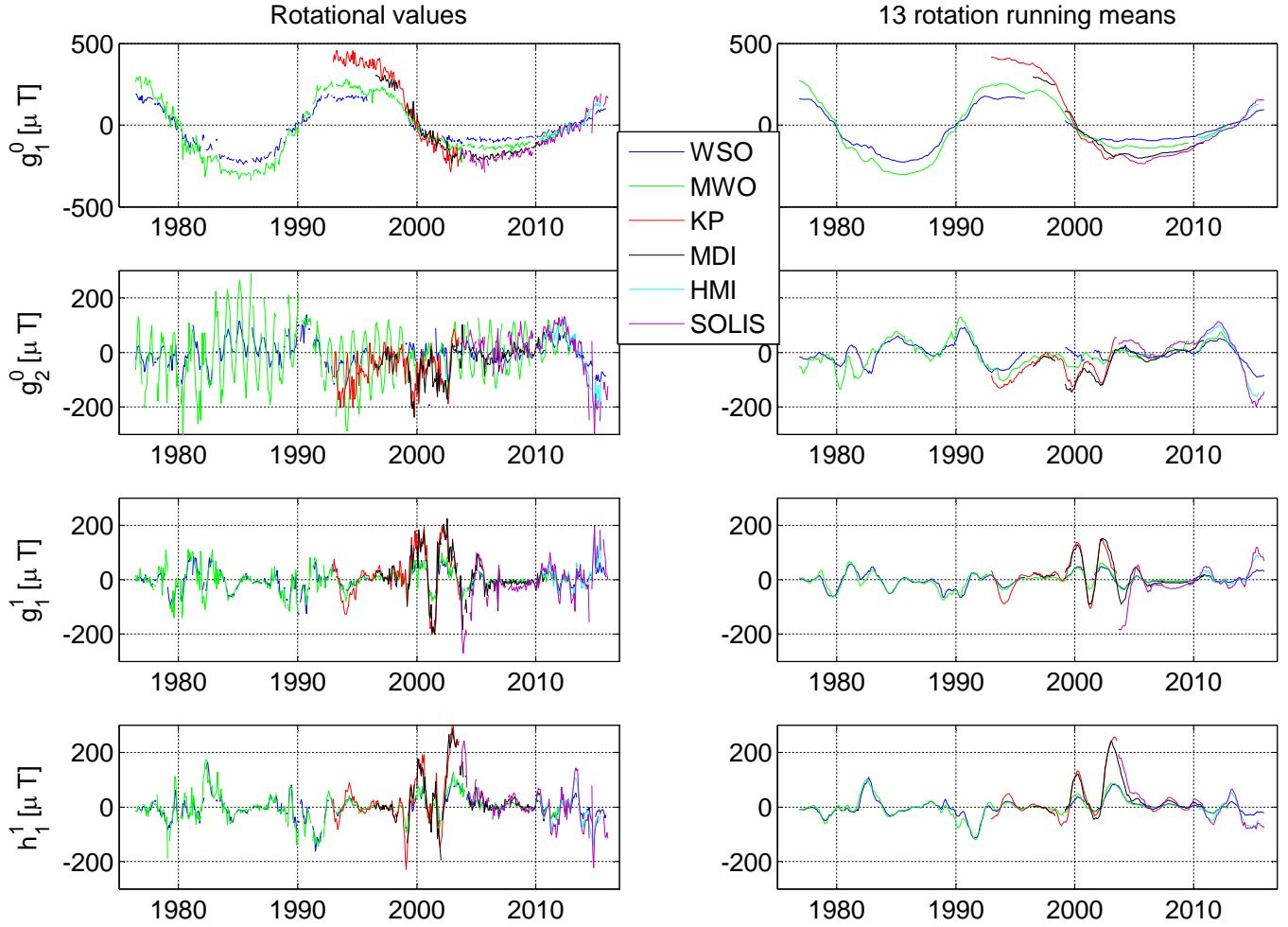
Fig. 1. First four harmonic coefficients. *Left*: rotational means; *right*: 13-rotation running means.

only 0.02. There are three clusters of points around WSO values of $-200\,\mu T$, $150\,\mu T$ and $-100\,\mu T$, which correspond to the polar fields of the minima of SC21, SC22, and SC 23. The scaling (regression) of the g_2^0 quadrupole term between WSO and MWO is much less uniform. The average scaling factor is 2.86 but the values are more scattered and error estimate 0.32 is much larger. This is due to several uncertainties in polar field observations discussed above, especially due to the vantage point effect and the related annual oscillation in g_2^0. Accordingly, the g_2^0 scaling factor of 2.86 from WSO to MWO is less reliable than the g_1^0 scaling, and includes a relatively much larger error. The two equatorial dipole terms g_1^1 and h_1^1 scale almost equally well as the axial dipole term with scaling factors of 1.23 and 1.18 but have roughly three times larger error than g_1^0. Since g_1^1 and h_1^1 are the sine and cosine components of the same harmonics, they should have the same scaling factor (at least for the long time interval studied here). The difference between the scaling factors of g_1^1 and h_1^1 indeed remains within the 2σ error of either scaling factor.

5. Scaling between the six data sets up to *n* = 9

5.1. Scaling between WSO and other data sets

Using the method depicted in Fig. 2 we now scale all the harmonic coefficients up to $n = 9$ between WSO and the other five

data sets. Upper panels of Fig. 3 show the scaling factors for g_n^m from WSO to the five data sets and lower panels show the related errors. Figure 3 shows only g_n^m; not h_n^m since g_n^m and h_n^m are the sine and cosine components of the same harmonic variables and show practically the same information, as demonstrated above for the equatorial dipole. Table 2 shows the values of the scaling factors and the related errors for all possible pairs of the six data sets up to $n = 2$. Appendix A includes Tables $A_1...A_{11}$ which give all the scaling factors and errors up to $n = 9$.

Figure 3 shows that all WSO to MWO scaling values remain rather small, mostly below 2. The even axial ($m = 0$) terms g_2^0, g_4^0, g_6^0 and g_8^0 are exceptions, which have larger scaling factors and larger errors. Scaling factors between WSO and KP are systematically larger and more variable than scaling factors between WSO and MWO. WSO to SOLIS scalings are relatively similar to WSO to KP scalings. Scaling factor for g_1^0 dipole from WSO to KP is 2.40 and from WSO to SOLIS 2.19, while higher harmonics indicate scaling factors even over 4 for both KP and SOLIS. The scaling factors between WSO and MDI show very large variations and generally increase with both m and n. Scaling factor for g_1^0 is 1.95, but g_2^0 term scaling cannot be determined for these two data sets because of an excessively large error (see Table 3). As seen in Fig. 1, MDI g_2^0 term is systematically negative in 1999–2004, in agreement with KP, but WSO and MWO indicate g_2^0 term around zero at that time.
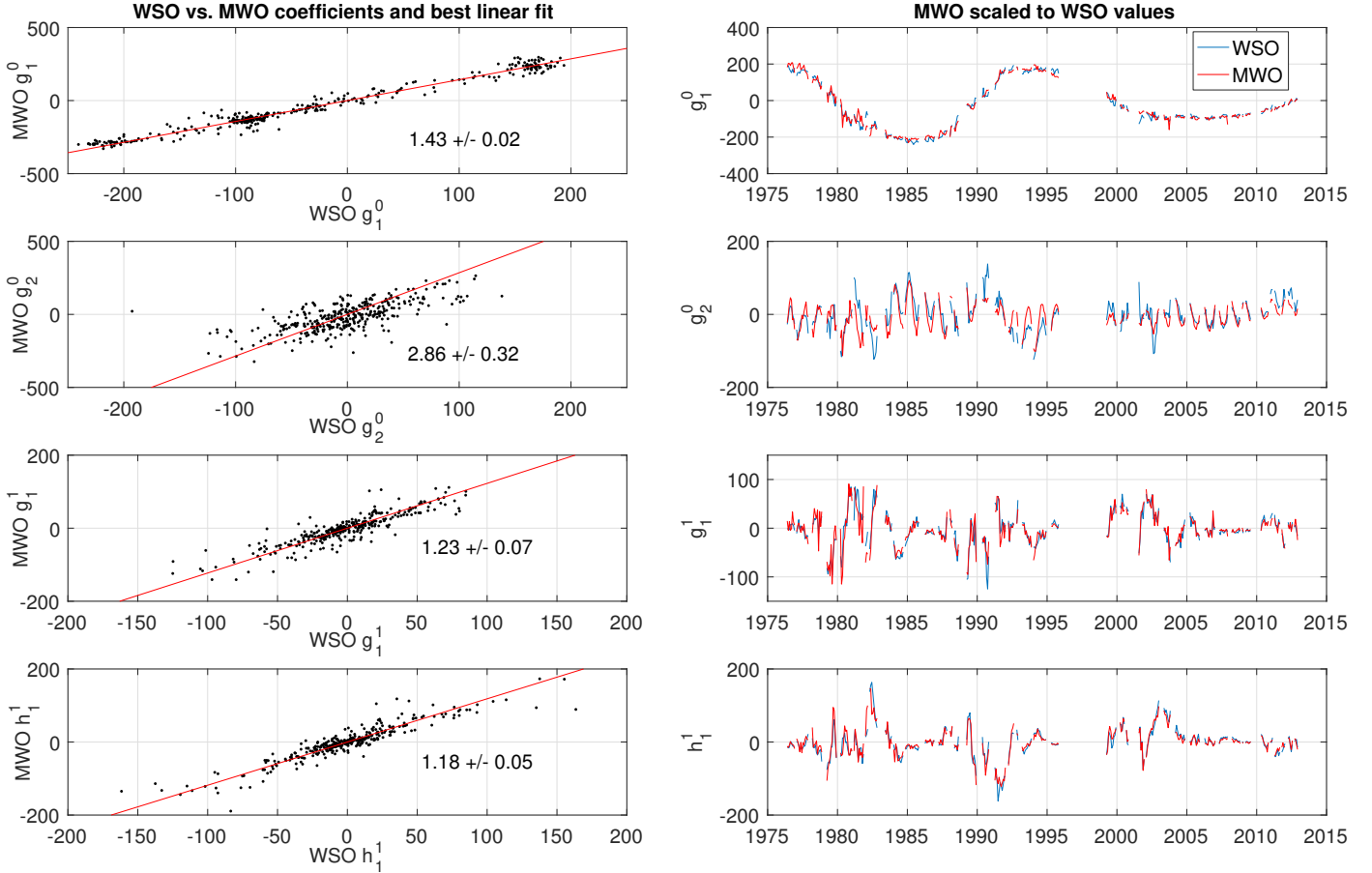
Fig. 2. *Left*: scatter plot of harmonic coefficients g_1^0, g_2^0, g_1^1 and h_1^1 between WSO and MWO data sets. *Right*: time series of harmonics, MWO values scaled to WSO according to coefficients in *the left panels*.

Table 2. Scaling factors for lowest harmonic brackets indicates that error is significantly larger than scaling factor.

Scaling	g_1^0	g_1^1	h_1^1	g_2^0	g_2^1	h_2^1	g_2^g	h_2^2
WSO to MWO	1.43 ± 0.02	1.23 ± 0.07	1.18 ± 0.05	2.85 ± 0.33	1.61 ± 0.06	1.69 ± 0.07	1.40 ± 0.04	1.48 ± 0.05
WSO to KP	2.40 ± 0.11	2.99 ± 0.17	3.05 ± 0.17	3.76 ± 0.86	3.51 ± 0.35	3.53 ± 0.26	3.31 ± 0.16	3.39 ± 0.28
WSO to SOLIS	2.24 ± 0.07	3.31 ±0.23	2.82 ± 0.19	2.58 ± 0.48	3.36 ± 0.25	3.20 ± 0.21	3.20 ± 0.13	3.55 ± 0.17
WSO to MDI	1.95 ± 0.04	3.12 ± 0.27	3.03 ± 0.22	(8.3 ± 403)	3.99 ± 0.36	3.86 ± 0.25	3.38 ± 0.18	3.28 ± 0.20
WSO to HMI	1.74 ± 0.13	2.26 ± 0.25	2.29 ± 0.19	1.85 ± 0.20	2.32 ± 0.25	2.22 ± 0.15	2.25 ± 0.16	2.57 ± 0.17
MWO to KP	1.70 ± 0.04	2.57 ± 0.15	2.61 ± 0.11	0.89 ± 0.42	2.15 ± 0.11	2.09 ± 0.09	2.28 ± 0.07	2.38 ± 0.09
MWO to SOLIS	1.50 ± 0.02	3.90 ± 0.48	3.24 ± 0.32	(0.41 ± 0.5)	2.01 ± 0.15	2.07 ± 0.15	2.53 ± 0.14	2.58 ± 0.14
MWO to MDI	1.36 ± 0.03	2.64 ± 0.16	2.54 ± 0.14	0.80 ± 0.40	2.33 ± 0.12	2.21 ± 0.09	2.43 ± 0.09	2.36 ± 0.14
MWO to HMI	1.23 ± 0.05	1.81 ± 0.37	2.17 ± 0.36	1.22 ± 0.20	1.41 ± 0.24	1.35 ± 0.14	1.53 ± 0.19	1.69 ± 0.18
KP to MDI	0.83 ± 0.03	1.00 ± 0.08	0.97 ± 0.06	1.09 ± 0.10	1.14 ± 0.07	1.08 ± 0.04	1.07 ± 0.05	1.03 ± 0.09
SOLIS to MDI	0.90 ± 0.005	0.56 ± 0.06	0.67 ± 0.05	0.36 ± 0.15	0.95 ± 0.06	0.86 ± 0.06	0.81 ± 0.05	0.77 ± 0.03
SOLIS to HMI	0.79 ± 0.05	0.76 ± 0.05	0.74 ± 0.06	0.81 ± 0.05	0.79 ± 0.05	0.72 ± 0.04	0.73 ± 0.05	0.79 ± 0.03

The scaling between WSO and HMI is particularly important. WSO is the longest and most homogenous ongoing series of observations, and several results based on WSO data, including the HCS tilt angle and source surface flux density, are widely used. Unfortunately there is an increasing risk of termination of WSO observations and, therefore, a need to reliably extend the WSO series using other observations, such as HMI data. Perhaps slightly surprisingly, these two instruments scale well, and the errors remain relatively small, typically smaller than for scaling factors between WSO and KP, SOLIS, or MDI. Axial dipole scaling factor from WSO to HMI is 1.74 ± 0.13. The scaling factor for the problematic g_2^0-term is 1.85 ± 0.20, which, within errors, is the same as the axial dipole scaling factor. The good

match in WSO to HMI g_2^0 scaling is probably due to large and systematically varying values of g_2^0 during the overlapping time 2010–2016 (see Fig. 1) when the vantage point effect was very weak. One also needs to have a correct zero-level in both instruments. The equatorial dipole scaling factors are slightly larger, 2.32 and 2.25, and scaling factors for higher harmonics increase relatively smoothly with n.

5.2. Scaling between other pairs of data sets

Upper panels (lower, respectively) of Fig. 4 show the scaling factors (their errors) between all other possible pairs of the six
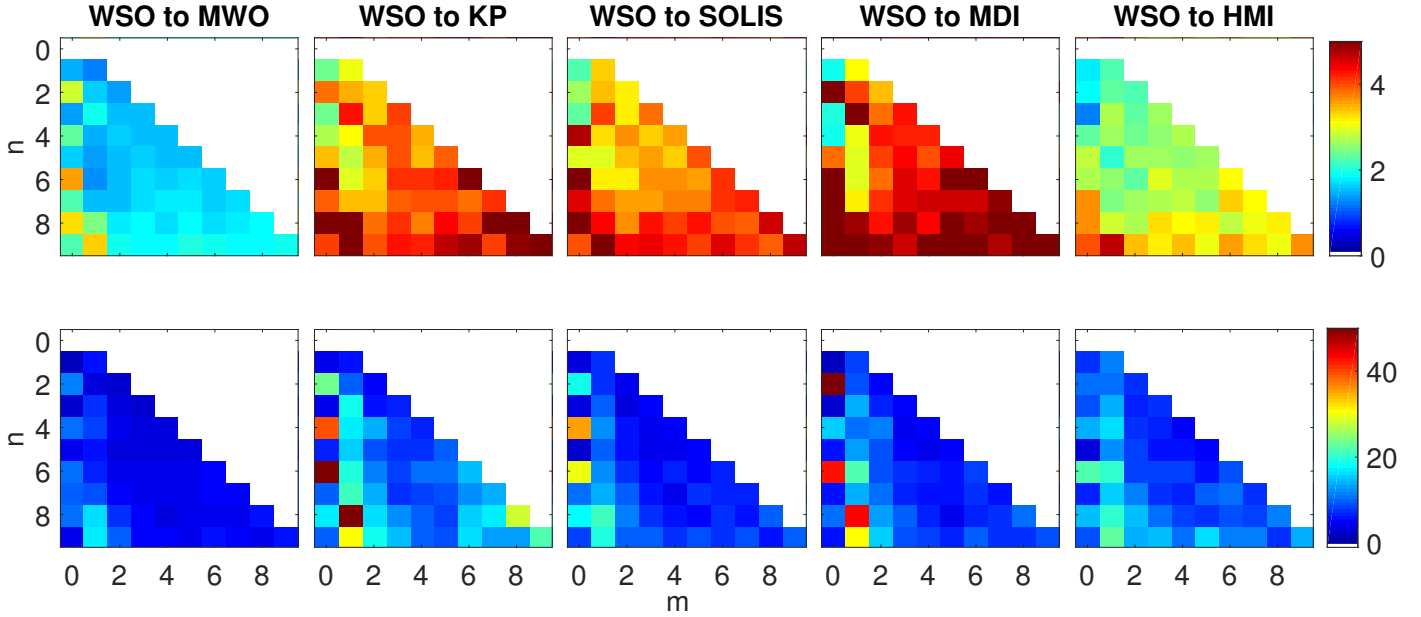
Fig. 3. Scaling factors for harmonics g_n^m from WSO to the five other data sets (*first row*), and the related relative (%) error estimates (*second row*). For accurate numeric values, we refer to Appendix A.
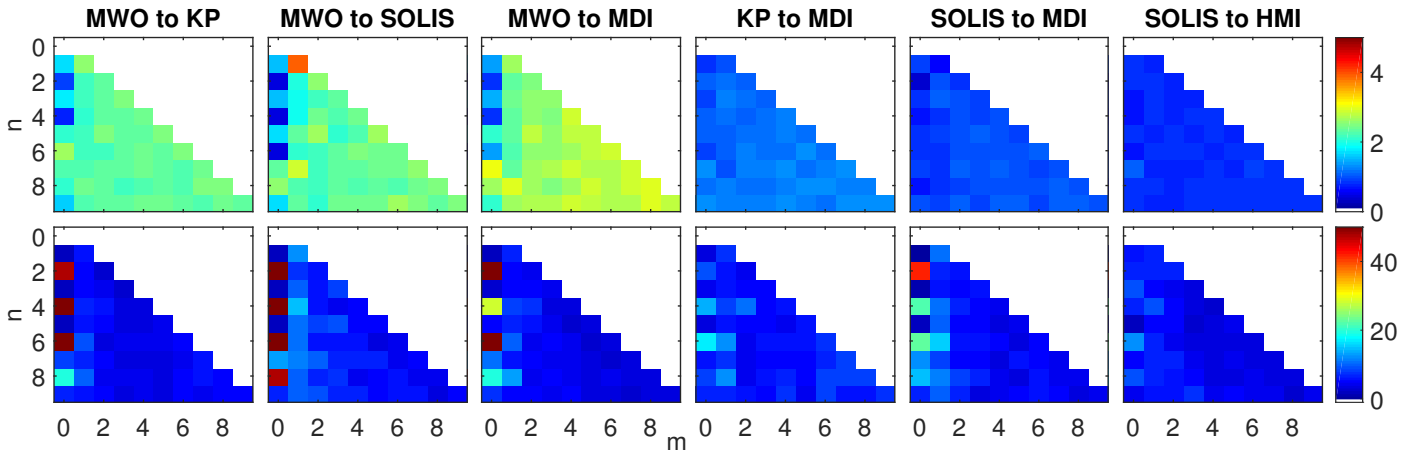

Fig. 4. Scaling factors for harmonics g_n^m from MWO to KP, MWO to SOLIS, MWO to MDI, KP to MDI, SOLIS to MDI, and SOLIS to HMI (*first row*), and the related relative (%) error estimates (*second row*). For accurate numeric values, we refer to Appendix A.

data sets: MWO versus KP, MWO versus SOLIS, MWO versus MDI, KP versus MDI, SOLIS versus MDI, and SOLIS versus HMI. We neglect the scalings for MWO to HMI, and MDI to HMI, since the overlaps between these pairings are too short for reliable comparison with this method. Figure 4 shows that in the case of MWO scalings, the errors for the even axial terms are so large (>50%) that these scaling factors cannot be considered reliable. This is a consequence of the large annual variation in MWO data due to the b_0-angle effect. However, the errors of MWO scalings for other harmonics are somewhat smaller than the corresponding WSO scalings. Scaling factor for g_1^0 from MWO to KP is 1.70, from MWO to SOLIS 1.48 and from MWO to MDI 1.36. For higher g_n^m terms the scaling factors are systematically larger and typically increase with m and n. Scalings from KP to MDI are almost independent of harmonic degree but the largest relative errors are found again for even axial terms. The scaling of the g_2^0 term for SOLIS to MDI is also unreliable, but all other scalings from SOLIS to MDI and SOLIS to HMI are reliable, fairly small and rather independent of harmonic degree.

The general pattern in Figs. 3 and 4 is that when scaling the lower resolution data to higher resolution data, the scaling factors typically increase with both m and n. The relative errors are comparatively small, especially for large m, but the axial ($m = 0$) terms, especially for even n, scale poorly. This is most likely related to the problems in zero-levels, polar field observations and possible polar field fillings as discussed above. Accordingly, the poorest-scaling low harmonic term is the g_2^0 term, which is very sensitive to inaccuracies in polar fields. This is especially true for scaling WSO to MDI and MWO to SOLIS, and therefore the corresponding scaling factors in Table 2 are in brackets.

6. Scaling of very high harmonics

Figure 5 shows the scaling factors up to $n = 180$ for the same pairs of high-resolution data sets as Fig. 4. The general pattern remains similar as for low harmonics: when scaling lower-resolution data to higher-resolution data, the scaling factors typically increase with both n and m. Typically scaling factors and
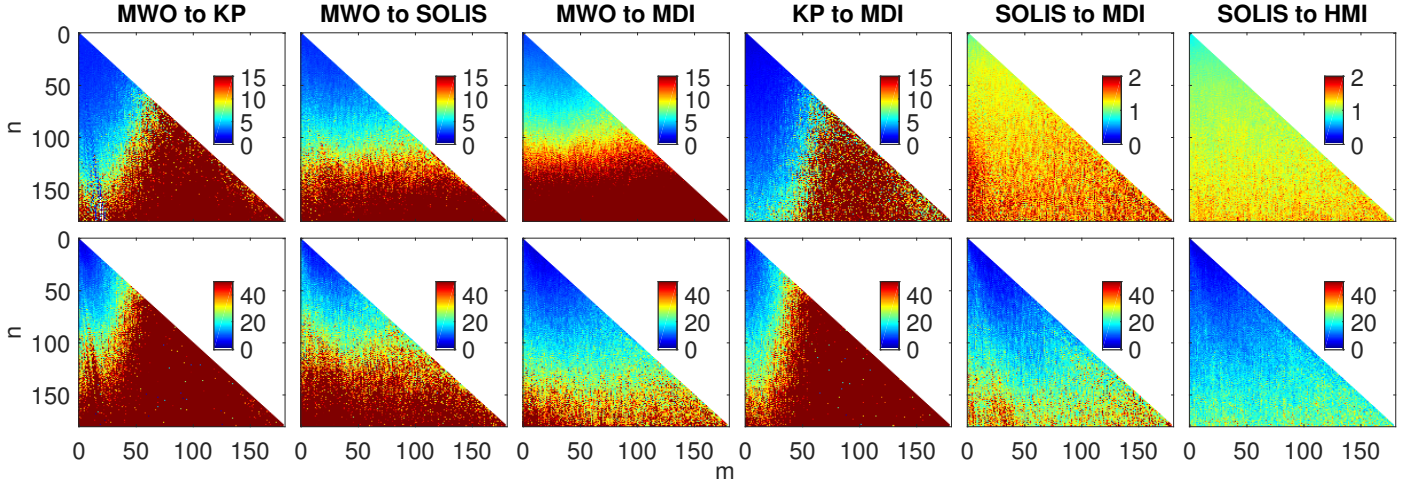
Fig. 5. Scaling factors for harmonics g_n^m from MWO to KP, MWO to SOLIS, MWO to MDI, KP to MDI, SOLIS to MDI, and SOLIS to HMI up to the $n = 180$ (*first row*), and the related relative (%) error estimates (*second row*). We note that in the *first row panels* 1–4 from left color-scale is from 0 to 15 and in *first panels* 5–6 color-scale is from 0 to 2.

errors for constant n are roughly independent of m, except for KP, whose errors increase much more strongly with m than with n. This indicates that the longitudinal position of magnetic features is different in KP maps (than in MWO or MDI), but the latitudinal structure is roughly the same as in the other data sets, since errors remain relatively small with higher n and and m.

Scaling MWO to KP, SOLIS, or MDI, the errors increase to a higher level (approx. 30%) around $n = 90$, which is expected considering the observational resolution in MWO. Figure 4 shows the scaling factors for MWO to KP and SOLIS for low harmonics (except axial terms) are approximately 2–3. Figure 5 shows a relatively steady increase of scaling factors with increasing n, reaching roughly 4 until $n = 90$, that is, within reasonable errors. MWO to SOLIS shows larger scaling factors for the high n, small m terms than MWO to KP, which is probably a consequence of the higher resolution of SOLIS maps.

SOLIS to MDI scaling factors increase slowly with n but remain below 2 for all n and m. Errors of SOLIS to MDI scalings are relatively small at least up to $n = 100$. As we already pointed out, SOLIS and HMI scale very well in the case of low harmonics (Fig. 4), and high harmonics do not change this result. The scaling factors for terms up to $n = 180$ slowly increase from approximately 0.7 to 1.3. Related errors increase with n, but are still smaller than for any other pairings of the six data sets.

7. Discussion

Several methods have already been used to scale the observed photospheric magnetic fields between different instruments. Svalgaard et al. (1978) introduced a single scaling coefficient for WSO observations in order to correct WSO data for magnetograph saturation (not to scale the WSO data to the same level with other data sets). Ulrich (1992) compared observations using two spectral lines and assumed that the line with a smaller saturation would better represent the strong magnetic field. They derived the latitude dependent scaling factors for MWO data, which were later used, for example, when deriving the source surface open magnetic flux (Wang & Sheeley 1995). On the other hand, histogram methods (Wenzler et al. 2006) give a good statistical correspondence between original full-disk observations, which is essential, for example, for TSI models. Riley et al. (2014) used the histogram method to study

scaling in different latitude bins, but did not find significant latitudinal dependence in scaling. The scaling factors they derived were relatively large. Over the studied period of Carrington rotations 1913–2126 the rotational scaling factors from WSO to MWO, for example, were 2.2–5.6 and from MWO to MDI 4.50–7.74. Pixel-by-pixel scaling is useful and can describe the statistical correspondence between observations, but requires that both data sets have roughly the same resolution (Pietarila et al. 2013).

In pixel-by-pixel, disk-integrated or histogram scaling methods, the active regions with intense magnetic fields have a larger impact on scaling factors than weak fields. Weak fields can be studied separately, but the weak field comparison is often questionable if the noise level is larger than the measured magnetic field (Pietarila et al. 2013). As a result, scaling factors based on the above methods are in general larger than scaling factors for low harmonics shown in this paper. Pixel-by-pixel comparison between SOLIS and HMI using full-disk observations on 14.11.2011 gives scaling factors from 1.4 (weak fields) to 0.7 (strong fields), thus significantly dependent upon field strength.

The benefit of the novel scaling method presented in this paper is that it gives an independent scaling factor for the different harmonic terms. The method applies to all synoptic maps and can be used to compare data sets of different resolutions. The new scaling method is superior, for example, when using the harmonic coefficients and the potential field source surface or any other coronal model to calculate the coronal magnetic field. With the scaled harmonic coefficients one can derive the scaled potential field approximation for the global magnetic field from the photosphere up to the coronal source surface and have closely similar field intensities from all data sets. These results will be presented in a separate publication (Virtanen & Mursula (in prep.)).

We found that the scaling factors for the axial dipole term g_1^0 for the many different pairs of data sets vary from 0.79 (SOLIS to HMI) to 2.24 (WSO to SOLIS). The g_1^0-term (shown in Fig. 1) has the largest intensity in SOLIS and the smallest in WSO, which implies that the polar fields are strongest in SOLIS and weakest in WSO. Errors are, in general, relatively small in all g_1^0 scalings.

When scaling WSO to other data sets, the corresponding scaling factors for the g_2^0 term are roughly equal (within error)

or larger than g_1^0 scaling factors (see Table 2). On the other hand, when scaling MWO to other data sets, the g_2^0 scalings are not larger than g_1^0 scaling factors, but the related errors are large. In the case of WSO to MDI and MWO to SOLIS the errors in g_2^0 scaling are larger than the scaling factors, which invalidates the scaling. Scaling factors for the g_2^0 term for pairs of higher-resolution data sets do not generally deviate from the g_1^0 scaling factors as much as in the case of lower-resolution MWO and WSO data. The vantage point effect, which mainly affects the g_2^0 term, weakens the quality of the g_2^0 scalings between the different data sets. The vantage point effect is strongest in MWO data, but has the same phase as in WSO (see Fig. 1). Therefore WSO to MWO g_2^0 scaling can be determined relatively reliably. However, as a consequence of the applied pole filling, the vantage point effect has an opposite phase in KP and SOLIS compared to MWO and WSO, leading to larger errors in g_2^0 scalings between these two sets of instruments. In MDI, the vantage point effect is relatively small but the g_2^0 scaling, especially with WSO (less with MWO), is very poor due to differing g_2^0 values in the early 2000s (see Fig. 1). Accordingly, their mutual differences are not mainly due to the vantage point effect. Also the other even axial harmonics ($m = 0$, $n = 4, 6, 8...$) between most pairs of data sets scale poorly. In addition to the vantage point effect and pole filling, problems with the zero-level of observations also affect these scalings, since even axial terms are very sensitive to zero-level errors.

Scaling factors for the two equatorial dipole terms (g_1^1 and h_1^1) are closely similar to each other. This is valid for all data sets. In most cases (except when scaling WSO to MWO and SOLIS to MDI/HMI), the equatorial dipole scaling factors are larger than the axial dipole scaling factors, most likely due to the saturation of strong fields in the low-resolution data sets. SOLIS scalings to HMI are almost the same for both axial and equatorial dipoles. In fact, SOLIS and HMI scale so well that all harmonics have closely similar scalings. Thus, one single overall scaling factor would be very reasonable between these two data sets.

The highest harmonic term that is scalable depends on the resolution of the data sets compared. In the best case of scaling SOLIS to HMI, the relative errors remain fairly small until approximately $n = 180$ and do not have significant dependence on m. This shows that SOLIS and HMI synoptic maps depict similar magnetic field structures up to the resolution of $1°$ in latitude/longitude. When scaling KP observation to MWO or MDI, errors increase faster with m and scaling factors become insignificant around $m = 50$, corresponding to the resolution of $3.6°$. However, interestingly, scalings for harmonic terms with large n but small m remain significant until approximately $n = 100$. This indicates some kind of longitudinal offset in KP synoptic maps.

When scaling low-resolution data to high-resolution data, the scaling factors for the equatorial dipole and higher harmonic terms are larger than for the axial dipole, supporting larger scaling for low-latitude fields Ulrich (1992). This is at least partly a consequence of magnetograph saturation, which is most significant in WSO data. On the other hand, the longitudinal width of active regions with most intense magnetic fields is typically approximately $10°$–$30°$, and thereby they only start to affect the harmonics above $m = 15$. Since different harmonics reflect different field structures, possible nonlinearities in observations can partly explain m-dependent scaling factors.

8. Conclusions

In this work we have studied the scaling of the photospheric magnetic field between six independent long-term data sets. We calculated the harmonic expansions of the magnetic field for all these data sets and investigated the scaling of the harmonic coefficients between all possible pairs of data sets. Different data sets generally scale to one another relatively well, with the exception of even axial terms, especially the g_2^0 quadrupole. Differences in polar field observations, pole filling, and data processing methods, as well as possible zero-level, mostly lead to a poor scaling between even axial terms.

We noted that the pole-filling methods of KP and SOLIS data make the phase of the annual vantage point effect change opposite to the phase in MWO and WSO data. On the other hand, MDI pole filling appears to reduce the vantage point effect relatively successfully. The mutual scaling between SOLIS and HMI is very good, and one single overall coefficient of approximately 0.8 would be a reasonable choice for those data sets, at least up to $m = 50$. The slight increase of scaling factors with increasing n may relate to different spatial resolutions and related filling factors. Still, the relative errors remain rather small at least up to the studies' 180th harmonic, verifying that SOLIS and HMI synoptic maps depict similar magnetic field structures up to the resolution of $1°$ in latitude/longitude.

Scaling factors for the low harmonic coefficients were found to be, in general, smaller than the scaling factors based on pixel-by-pixel comparison or histogram techniques. This indicates that a significant amount of total flux in high-resolution data is contained in high harmonics that are beyond the resolution of, for example, WSO observations. Scaling factors between harmonic coefficients depend on the order of the harmonic term. The relative contribution of the different harmonic terms to the field intensity at different latitudes varies in time. We note that if one would scale synoptic maps before solving harmonic coefficients, scaling factors should be nonlinear, as well as time and latitude dependent in order to reach the same potential field solution.

Results in this paper show that comparing harmonic terms between two data sets yields a simple and accurate scaling. We note that a correct scaling for the lowest few ($n \leq 3$) harmonics is most essential for coronal modeling, since the lowest harmonics are the most important for coronal and heliospheric magnetic fields. Another benefit of the harmonic scaling is that it can be applied, without any changes in resolution, to all possible data sets of any resolution.

References

Altschuler, M. D., & Newkirk, G. 1969, Sol. Phys., 9, 131

Arge, C. N., & Pizzo, V. J. 2000, J. Geophys. Res., 105, 10465

Arge, C. N., Henney, C. J., Koller, J., et al. 2010, Twelfth International Solar Wind Conference, 1216, 343

Babcock, H. W. 1953, ApJ, 118, 387

Berger, T., & Lites, B. 2003, Sol. Phys., 213, 213

Hale, G. E. 1908, ApJ, 28, 315

Harvey, J., & Munoz-Jaramillo, A. 2015, in AAS/AGU Triennial Earth-Sun Summit, http://nisp.nso.edu/sites/nisp.nso.edu/files/images/poster/spd2015/jh.pdf, 11102

Hoeksema, J. T. 1985, http://wso.stanford.edu/words/Description.ps

Hoeksema, J. T., Wilcox, J. M., & Scherrer, P. H. 1983, J. Geophys. Res., 88, 9910

Holappa, L., Mursula, K., & Asikainen, T. 2014, J. Geophys. Res. (Space Phys.), 119, 9407

Jolliffe, I. 2005, Principal Component Analysis (John Wiley & Sons, Ltd)

Koskela, J. S., Virtanen, I. I., & Mursula, K. 2017, ApJ, 835, 63

Lefèvre, L., & Clette, F. 2011, A&A, 536, L11

Liu, Y., Hoeksema, J. T., Scherrer, P. H., et al. 2012, Sol. Phys., 279, 295

Livingston, W., & Penn, M. 2009, EOS Transactions, 90, 257

Muñoz-Jaramillo, A., Senkpeil, R. R., Longcope, D. W., et al. 2015, ApJ, 804, 68

Mursula, K., & Hiltula, T. 2003, Geophys. Res. Lett., 30, 2135

Mursula, K., & Virtanen, I. I. 2011, A&A, 525, L12

Petrie, G. J. D. 2015, Liv. Rev. Sol. Phys., 12, 5

Pietarila, A., Bertello, L., Harvey, J. W., & Pevtsov, A. A. 2013, Sol. Phys., 282, 91

Riley, P., Ben-Nun, M., Linker, J. A., et al. 2014, Sol. Phys., 289, 769

Schatten, K. H., Wilcox, J. M., & Ness, N. F. 1969, Sol. Phys., 6, 442

Schrijver, C. J., & Liu, Y. 2008, Sol. Phys., 252, 19

Sun, X., Liu, Y., Hoeksema, J. T., Hayashi, K., & Zhao, X. 2011, Sol. Phys., 270, 9

Svalgaard, L., Duvall, Jr., T. L., & Scherrer, P. H. 1978, Sol. Phys., 58, 225

Tran, T., Bertello, L., Ulrich, R. K., & Evans, S. 2005, ApJS, 156, 295

Ulrich, R. K. 1992, in Cool Stars, Stellar Systems, and the Sun, eds. M. S. Giampapa, & J. A. Bookbinder, ASP Conf. Ser., 26, 265

Ulrich, R. K., & Tran, T. 2013, ApJ, 768, 189

Upton, L., & Hathaway, D. H. 2014, ApJ, 780, 5

Virtanen, I., & Mursula, K. 2016, A&A, 591, A78

Virtanen, I. I., & Mursula, K. 2014, ApJ, 781, 99

Wang, Y.-M. 2014, Space Sci. Rev., 186, 387

Wang, Y.-M., & Sheeley, Jr., N. R. 1995, ApJ, 447, L143

Wenzler, T., Solanki, S. K., Krivova, N. A., & Fröhlich, C. 2006, A&A, 460, 583

Zhao, X. P., Hoeksema, J. T., & Scherrer, P. H. 2005, J. Geophys. Res., 110, 10101

Appendix A: Scaling factors

Table A.1. Scaling factors from WSO to MWO.

n \ m	0	1	2	3	4	5	6	7	8	9
0	–									
0										
1	1.43 ± 0.02	1.23 ± 0.07								
2	2.85 ± 0.33	1.61 ± 0.06	1.40 ± 0.04							
3	1.37 ± 0.03	1.95 ± 0.14	1.52 ± 0.05	1.53 ± 0.04						
4	2.34 ± 0.25	1.46 ± 0.12	1.59 ± 0.06	1.51 ± 0.05	1.54 ± 0.05					
5	1.62 ± 0.07	1.38 ± 0.08	1.52 ± 0.05	1.59 ± 0.06	1.55 ± 0.05	1.54 ± 0.06				
6	3.56 ± 0.37	1.32 ± 0.08	1.50 ± 0.06	1.66 ± 0.07	1.62 ± 0.07	1.68 ± 0.07	1.61 ± 0.08			
7	2.23 ± 0.22	1.50 ± 0.13	1.52 ± 0.08	1.66 ± 0.07	1.73 ± 0.07	1.76 ± 0.07	1.58 ± 0.08	1.71 ± 0.08		
8	3.23 ± 0.35	2.49 ± 0.40	1.74 ± 0.13	1.84 ± 0.09	1.65 ± 0.06	1.82 ± 0.07	1.66 ± 0.08	1.78 ± 0.08	1.85 ± 0.10	
9	2.22 ± 0.09	3.29 ± 0.55	1.90 ± 0.19	1.86 ± 0.09	1.84 ± 0.09	2.00 ± 0.09	1.89 ± 0.11	1.85 ± 0.09	1.82 ± 0.07	1.88 ± 0.10

Table A.2. Scaling factors from WSO to KP.

n \ m	0	1	2	3	4	5	6	7	8	9
0	–									
0										
1	2.40 ± 0.11	2.99 ± 0.17								
2	3.76 ± 0.86	3.51 ± 0.35	3.31 ± 0.16							
3	2.40 ± 0.11	4.28 ± 0.80	3.31 ± 0.19	4.04 ± 0.28						
4	2.73 ± 1.07	3.07 ± 0.51	3.92 ± 0.52	3.96 ± 0.32	3.51 ± 0.24					
5	3.43 ± 0.21	2.80 ± 0.43	3.50 ± 0.31	3.91 ± 0.29	3.41 ± 0.25	3.89 ± 0.38				
6	9.34 ± 42.99	2.91 ± 0.57	3.28 ± 0.36	4.12 ± 0.35	4.11 ± 0.43	4.18 ± 0.43	4.95 ± 0.73			
7	3.90 ± 0.38	3.38 ± 0.70	3.37 ± 0.47	3.84 ± 0.28	3.91 ± 0.32	3.98 ± 0.34	3.80 ± 0.45	4.11 ± 0.58		
8	5.20 ± 0.88	5.16 ± 48.69	3.82 ± 0.63	4.13 ± 0.50	3.72 ± 0.36	4.37 ± 0.34	4.01 ± 0.63	5.46 ± 0.92	6.76 ± 1.90	
9	3.99 ± 0.39	8.54 ± 2.61	3.96 ± 0.72	4.25 ± 0.62	4.15 ± 0.40	4.64 ± 0.40	4.82 ± 0.76	4.02 ± 0.53	4.90 ± 0.62	5.24 ± 1.15

Table A.3. Scaling factors from WSO to SOLIS.

n \ m	0	1	2	3	4	5	6	7	8	9
0	–									
0										
1	2.24 ± 0.07	3.31 ± 0.23								
2	2.58 ± 0.48	3.36 ± 0.25	3.20 ± 0.13							
3	2.29 ± 0.07	4.00 ± 0.39	3.13 ± 0.12	3.79 ± 0.18						
4	4.72 ± 1.66	3.22 ± 0.38	3.63 ± 0.21	3.30 ± 0.14	3.56 ± 0.17					
5	2.97 ± 0.08	2.90 ± 0.29	3.39 ± 0.20	3.53 ± 0.15	3.34 ± 0.13	3.95 ± 0.19				
6	5.58 ± 1.65	3.18 ± 0.40	3.15 ± 0.22	3.64 ± 0.18	3.64 ± 0.23	3.55 ± 0.16	4.09 ± 0.28			
7	4.53 ± 0.48	3.78 ± 0.52	3.56 ± 0.34	3.59 ± 0.20	3.73 ± 0.17	3.75 ± 0.26	4.08 ± 0.26	4.20 ± 0.27		
8	6.13 ± 1.08	4.33 ± 0.91	3.64 ± 0.42	4.28 ± 0.31	4.03 ± 0.23	4.22 ± 0.22	3.97 ± 0.28	3.85 ± 0.23	4.55 ± 0.45	
9	3.95 ± 0.34	7.04 ± 1.38	4.35 ± 0.43	4.38 ± 0.42	4.26 ± 0.30	4.06 ± 0.37	4.51 ± 0.35	4.11 ± 0.37	3.88 ± 0.22	4.62 ± 0.44

Table A.4. Scaling factors from WSO to MDI.

n \ m	0	1	2	3	4	5	6	7	8	9
0	–									
0										
1	1.95 ± 0.04	3.12 ± 0.27								
2	8.25 ± 403.05	3.99 ± 0.36	3.38 ± 0.18							
3	2.02 ± 0.05	5.13 ± 0.68	3.83 ± 0.26	4.29 ± 0.22						
4	1.95 ± 0.30	3.01 ± 0.31	4.25 ± 0.47	4.15 ± 0.19	4.18 ± 0.19					
5	3.78 ± 0.23	2.95 ± 0.38	4.03 ± 0.35	4.37 ± 0.21	3.96 ± 0.16	4.41 ± 0.20				
6	5.52 ± 2.35	2.92 ± 0.62	3.79 ± 0.33	4.46 ± 0.32	4.26 ± 0.27	4.97 ± 0.30	5.20 ± 0.41			
7	5.21 ± 0.29	3.19 ± 0.44	4.10 ± 0.45	4.51 ± 0.30	4.55 ± 0.25	4.58 ± 0.27	4.55 ± 0.32	4.87 ± 0.29		
8	5.12 ± 0.55	4.83 ± 2.11	4.28 ± 0.57	4.82 ± 0.48	4.33 ± 0.29	5.43 ± 0.25	4.80 ± 0.33	5.44 ± 0.41	5.89 ± 0.62	
9	5.06 ± 0.28	10.80 ± 3.27	4.91 ± 0.74	4.56 ± 0.40	4.94 ± 0.41	5.39 ± 0.34	5.12 ± 0.51	4.76 ± 0.35	5.37 ± 0.39	5.44 ± 0.47

Table A.5. Scaling factors from WSO to HMI.

n \ m	0	1	2	3	4	5	6	7	8	9
0	–									
0										
1	1.74 ± 0.13	2.26 ± 0.25								
2	1.85 ± 0.20	2.32 ± 0.25	2.25 ± 0.16							
3	1.25 ± 0.11	2.71 ± 0.36	2.29 ± 0.15	2.64 ± 0.18						
4	2.34 ± 0.32	2.64 ± 0.42	2.41 ± 0.17	2.55 ± 0.17	2.67 ± 0.14					
5	2.78 ± 0.09	2.09 ± 0.26	2.62 ± 0.22	2.61 ± 0.14	2.51 ± 0.14	2.60 ± 0.13				
6	2.70 ± 0.59	2.58 ± 0.52	2.30 ± 0.18	2.94 ± 0.23	2.67 ± 0.21	2.70 ± 0.16	3.06 ± 0.28			
7	3.63 ± 0.23	2.43 ± 0.37	2.61 ± 0.29	2.72 ± 0.21	2.81 ± 0.18	2.54 ± 0.25	3.34 ± 0.35	3.09 ± 0.22		
8	3.60 ± 0.53	2.86 ± 0.56	2.73 ± 0.39	3.23 ± 0.33	3.08 ± 0.24	3.15 ± 0.23	2.78 ± 0.25	3.02 ± 0.24	3.16 ± 0.37	
9	3.95 ± 0.34	4.63 ± 1.05	3.36 ± 0.47	3.14 ± 0.45	3.42 ± 0.37	3.03 ± 0.49	3.54 ± 0.39	3.24 ± 0.36	3.04 ± 0.21	3.61 ± 0.51

Table A.6. Scaling factors from MWO to KP.

n \ m	0	1	2	3	4	5	6	7	8	9
0	–									
0										
1	1.70 ± 0.04	2.57 ± 0.15								
2	0.89 ± 0.42	2.15 ± 0.11	2.28 ± 0.07							
3	1.74 ± 0.04	2.13 ± 0.10	2.32 ± 0.09	2.43 ± 0.07						
4	0.76 ± 0.84	2.11 ± 0.15	2.30 ± 0.13	2.27 ± 0.08	2.38 ± 0.09					
5	2.05 ± 0.04	2.12 ± 0.12	2.47 ± 0.11	2.31 ± 0.08	2.34 ± 0.07	2.44 ± 0.10				
6	2.59 ± 18.86	2.15 ± 0.18	2.17 ± 0.08	2.33 ± 0.10	2.39 ± 0.10	2.29 ± 0.09	2.47 ± 0.12			
7	2.23 ± 0.18	2.21 ± 0.15	2.27 ± 0.12	2.27 ± 0.08	2.42 ± 0.09	2.29 ± 0.08	2.21 ± 0.09	2.37 ± 0.13		
8	2.09 ± 0.41	2.36 ± 0.23	2.27 ± 0.09	2.19 ± 0.09	2.23 ± 0.09	2.33 ± 0.08	2.24 ± 0.12	2.46 ± 0.14	2.44 ± 0.13	
9	1.61 ± 0.11	2.25 ± 0.14	2.29 ± 0.11	2.28 ± 0.08	2.36 ± 0.10	2.36 ± 0.08	2.34 ± 0.12	2.21 ± 0.09	2.40 ± 0.11	2.33 ± 0.12

Table A.7. Scaling factors from MWO to SOLIS.

n \ m	0	1	2	3	4	5	6	7	8	9
0	–									
0										
1	1.50 ± 0.02	3.90 ± 0.48								
2	0.41 ± 0.49	2.01 ± 0.15	2.53 ± 0.14							
3	1.56 ± 0.02	1.92 ± 0.18	2.15 ± 0.12	2.34 ± 0.19						
4	0.04 ± 0.22	1.89 ± 0.28	2.35 ± 0.14	2.26 ± 0.10	2.41 ± 0.12					
5	1.71 ± 0.03	2.34 ± 0.25	2.61 ± 0.21	2.05 ± 0.18	2.24 ± 0.12	2.59 ± 0.13				
6	0.45 ± 0.69	2.10 ± 0.23	2.14 ± 0.12	2.28 ± 0.14	2.42 ± 0.14	2.41 ± 0.08	2.39 ± 0.10			
7	2.28 ± 0.30	2.85 ± 0.32	2.19 ± 0.21	2.30 ± 0.15	2.34 ± 0.16	2.36 ± 0.16	2.35 ± 0.11	2.57 ± 0.13		
8	2.56 ± 1.20	2.24 ± 0.22	2.16 ± 0.15	2.30 ± 0.17	2.22 ± 0.10	2.31 ± 0.11	2.26 ± 0.13	2.35 ± 0.09	2.48 ± 0.09	
9	1.69 ± 0.12	2.32 ± 0.22	2.05 ± 0.19	2.38 ± 0.16	2.36 ± 0.15	2.38 ± 0.11	2.58 ± 0.15	2.45 ± 0.15	2.29 ± 0.08	2.47 ± 0.12

Table A.8. Scaling factors from MWO to MDI.

n \ m	0	1	2	3	4	5	6	7	8	9
0	–									
0										
1	1.36 ± 0.03	2.64 ± 0.16								
2	0.80 ± 0.40	2.33 ± 0.12	2.43 ± 0.09							
3	1.41 ± 0.04	2.40 ± 0.12	2.53 ± 0.12	2.52 ± 0.11						
4	0.78 ± 0.22	2.27 ± 0.18	2.53 ± 0.18	2.48 ± 0.08	2.81 ± 0.10					
5	2.06 ± 0.10	2.27 ± 0.14	2.76 ± 0.15	2.57 ± 0.10	2.75 ± 0.07	2.77 ± 0.09				
6	1.40 ± 0.76	2.19 ± 0.21	2.56 ± 0.11	2.53 ± 0.12	2.61 ± 0.10	2.77 ± 0.08	2.82 ± 0.10			
7	2.98 ± 0.32	2.34 ± 0.13	2.65 ± 0.14	2.67 ± 0.11	2.86 ± 0.12	2.66 ± 0.09	2.69 ± 0.08	2.89 ± 0.09		
8	2.61 ± 0.50	2.93 ± 0.38	2.64 ± 0.11	2.48 ± 0.12	2.60 ± 0.10	2.82 ± 0.10	2.73 ± 0.11	2.82 ± 0.09	2.89 ± 0.10	
9	2.05 ± 0.15	2.64 ± 0.14	2.70 ± 0.14	2.68 ± 0.10	2.83 ± 0.15	2.78 ± 0.09	2.70 ± 0.09	2.73 ± 0.08	2.92 ± 0.09	2.79 ± 0.08

Table A.9. Scaling factors from KP to MDI.

n \ m	0	1	2	3	4	5	6	7	8	9
0	–									
0										
1	0.83 ± 0.03	1.00 ± 0.08								
2	1.09 ± 0.10	1.14 ± 0.07	1.07 ± 0.05							
3	0.87 ± 0.04	1.21 ± 0.07	1.10 ± 0.05	1.06 ± 0.05						
4	1.05 ± 0.14	1.17 ± 0.10	1.04 ± 0.11	1.11 ± 0.06	1.19 ± 0.07					
5	1.09 ± 0.04	1.06 ± 0.06	1.11 ± 0.05	1.14 ± 0.06	1.22 ± 0.05	1.17 ± 0.07				
6	0.93 ± 0.16	1.04 ± 0.12	1.19 ± 0.05	1.13 ± 0.06	1.12 ± 0.07	1.26 ± 0.08	1.14 ± 0.09			
7	1.29 ± 0.07	1.01 ± 0.07	1.17 ± 0.05	1.17 ± 0.06	1.27 ± 0.07	1.16 ± 0.06	1.24 ± 0.09	1.31 ± 0.10		
8	1.13 ± 0.09	1.24 ± 0.15	1.16 ± 0.05	1.16 ± 0.07	1.25 ± 0.08	1.26 ± 0.07	1.26 ± 0.10	1.17 ± 0.09	1.25 ± 0.10	
9	1.27 ± 0.09	1.20 ± 0.08	1.19 ± 0.07	1.20 ± 0.06	1.26 ± 0.09	1.18 ± 0.05	1.16 ± 0.10	1.27 ± 0.07	1.27 ± 0.08	1.29 ± 0.10

Table A.10. Scaling factors from SOLIS to MDI.

n \ m	0	1	2	3	4	5	6	7	8	9
0	–									
0										
1	0.90 ± 0.00	0.56 ± 0.06								
2	0.36 ± 0.15	0.95 ± 0.06	0.81 ± 0.05							
3	0.85 ± 0.01	1.07 ± 0.07	0.96 ± 0.05	0.89 ± 0.05						
4	0.68 ± 0.15	0.82 ± 0.09	0.99 ± 0.07	0.92 ± 0.04	1.00 ± 0.05					
5	0.79 ± 0.01	0.92 ± 0.09	0.95 ± 0.05	1.02 ± 0.05	0.99 ± 0.03	0.92 ± 0.03				
6	0.85 ± 0.19	0.85 ± 0.13	0.94 ± 0.06	0.94 ± 0.05	0.98 ± 0.03	1.02 ± 0.05				
7	0.86 ± 0.10	0.80 ± 0.07	1.02 ± 0.05	1.00 ± 0.05	1.02 ± 0.04	1.01 ± 0.06	0.92 ± 0.04	0.97 ± 0.04		
8	0.70 ± 0.10	0.80 ± 0.09	0.93 ± 0.08	1.01 ± 0.07	1.01 ± 0.04	0.99 ± 0.03	1.01 ± 0.06	1.04 ± 0.04	0.95 ± 0.04	
9	0.95 ± 0.06	0.87 ± 0.08	1.06 ± 0.07	0.91 ± 0.03	1.05 ± 0.05	1.06 ± 0.05	0.91 ± 0.05	1.03 ± 0.05	1.03 ± 0.03	0.97 ± 0.04

Table A.11. Scaling factors from SOLIS to HMI.

n \ m	0	1	2	3	4	5	6	7	8	9
0	–									
0										
1	0.79 ± 0.05	0.76 ± 0.05								
2	0.81 ± 0.05	0.79 ± 0.05	0.73 ± 0.05							
3	0.63 ± 0.06	0.78 ± 0.04	0.76 ± 0.03	0.76 ± 0.02						
4	0.70 ± 0.05	0.83 ± 0.07	0.76 ± 0.04	0.78 ± 0.03	0.79 ± 0.02					
5	0.81 ± 0.01	0.75 ± 0.04	0.79 ± 0.04	0.77 ± 0.02	0.80 ± 0.03	0.77 ± 0.03				
6	0.68 ± 0.08	0.78 ± 0.05	0.78 ± 0.03	0.82 ± 0.03	0.78 ± 0.03	0.80 ± 0.03	0.83 ± 0.03			
7	1.02 ± 0.05	0.77 ± 0.05	0.77 ± 0.05	0.76 ± 0.03	0.81 ± 0.03	0.78 ± 0.04	0.87 ± 0.03	0.81 ± 0.03		
8	0.85 ± 0.08	0.84 ± 0.05	0.78 ± 0.05	0.81 ± 0.04	0.80 ± 0.03	0.81 ± 0.03	0.82 ± 0.03	0.83 ± 0.03	0.86 ± 0.03	
9	0.81 ± 0.04	0.76 ± 0.05	0.77 ± 0.04	0.81 ± 0.06	0.82 ± 0.04	0.81 ± 0.04	0.85 ± 0.03	0.84 ± 0.04	0.82 ± 0.02	0.84 ± 0.03